

A robust method for inverse halftoning via two-dimensional nonlinear pyramid

Yueping Kong (孔月萍)^{1,2} and Ping Zeng (曾平)¹

¹Research Institute of Computer Peripherals, Xidian University, Xi'an 710071

²College of Information and Control, Xi'an University of Architecture and Technology, Xi'an 710055

Received March 13, 2007

Based on the principle of spatial pyramid for signal, a multi-scale transform of two-dimensional (2D) interpolating pyramid is constructed by the nonlinear median operator. The transform properties of error diffuse halftoning noise on multiple scales are investigated and analyzed through experiments. According to these properties, a robust inverse halftoning method is proposed. The halftoning image is firstly pre-processed by a Gaussian low-pass filter, and decomposed by the one-scale transform. Then a Wiener filter is employed to the detailed coefficients. Finally an inverse image is reconstructed. Experimental results show that the proposed transform has the advantage of separating the halftoning noise and image detail over linear multi-resolution transform. The presented inverse halftoning method performs some excellent abilities on sharp edge, high peak signal-to-noise ratio (PSNR), and small memory requirement.

OCIS codes: 100.2810, 350.6980, 330.6130, 100.2000.

The process of rendition from continuous-tone images into a medium on which only two levels can be displayed is defined as digital halftoning^[1]. It has become important with the availability and adoption of bi-level devices such as facsimile machine and plasma display. Inverse halftoning is a reconstruction process of retrieving the continuous-tone image from its halftoned version. The applications of inverse halftoning can be found in diverse areas of image compression, enhancement, scaling and other processing on printed and facsimile images. In these applications, image processing operations cannot be directly performed on the image, and inverse halftoning is essential^[2].

The error diffuse (ED) halftoning is a nonlinear system that has been proved by Ulichney^[1], which only introduces blue noise to halftoned image on median and high frequencies. Simple smoothing means edges will be reduced. Many different techniques are used to reconstruct the inverse halftoning, including machine learning^[2,3], adaptive iteration^[4], maximum *a posteriori* (MAP) estimation^[5], nonlinear filtering^[6], and edge enhancement^[6,7]. But the iteration process and MAP estimation involve more complex computation. And the enhancement method will generate the illusive edges in result when the image is halftoned by a bigger or hexagonal ED kernel. Focusing on the nonlinear feature of ED system, two-dimensional median interpolating pyramid transform (2D-MIPT) is presented. Using this nonlinear pyramid transform, halftone noise can be separated effectively. Furthermore, we propose a robust inverse halftoning method for ED halftoning.

The Laplacian pyramid transform has been introduced by Burt *et al.* and applied on image coding^[8]. The iteration process of decomposition and reconstruction in one-dimensional (1D) case is given in Fig. 1. Usually the low-pass filters (LPFs) of W and W' are linear^[8,9], but they may also be nonlinear. Donoho *et al.* discussed a special nonlinear refinement scheme to replace the stationary linear scheme for wavelet transforms^[10].

The refinement scheme is based on polynomials which come from the interpolating median function of the underlying object. It is deployed in multi-resolution fashion to construct nonlinear MIPT, and it has associated forward and inverse transforms. Donoho's results show that nonlinear pyramid has a very different performance compared with traditional wavelets when it copes with non-Gaussian data. And it is effective to separate and remove the Cauchy noise. Now we consider to make a little change along with Refs. [10,11] to build the 2D-MIPT.

We define the median operator as follows. Given integers y_1, y_2, \dots, y_a , and let $y_1 \leq y_2 \leq \dots \leq y_a$, then the median operator is denoted as

$$\text{median}\{y_1, y_2, \dots, y_a\} = \begin{cases} y_{b+1}, & a = 2b + 1; \\ (y_b + y_{b+1})/2, & a = 2b. \end{cases} \quad (1)$$

Assuming that $x^0(m, n)$ is an original image, $\psi^k \uparrow$ represents the 2D-MIPT decomposition operator of $x^k \rightarrow x^{k+1}$ which transforms x^0 to a sequence of lower spatial resolution $\{x^1, x^2, x^3, \dots\}$, and the lost detailed information from $x^k \rightarrow x^{k+1}$ is represented as $\{d^1, d^2, d^3, \dots\}$. Correspondingly, $\psi^k \downarrow$ represents the reconstruction operator of $x^{k+1} \rightarrow x^k$ with $\{x^1, x^2, x^3, \dots\}$ and $\{d^1, d^2, d^3, \dots\}$. Under these identifiers, the forward and inverse 2D-MIPTs can be described as

$$\psi^k \uparrow: x^{k+1}(m, n) = \text{median}\{x^k(2m+i, 2n+j) | (i, j) \in W_{i,j}^b\}, \quad (2)$$

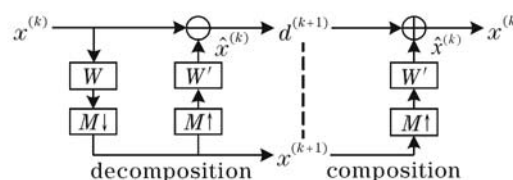


Fig. 1. Structure of pyramid decomposition and reconstruction.

$$\psi^k \downarrow: \hat{x}^k(2m, 2n) = \text{median}\{x^{k+1}(m, n)\}, \quad (3)$$

$$\begin{aligned} \hat{x}^k(2m, 2n+1) &= \text{median}\{x^{k+1}(m-1, n), x^{k+1}(m, n), \\ &x^{k+1}(m+1, n), x^{k+1}(m-1, n+1), \\ &x^{k+1}(m, n+1), x^{k+1}(m+1, n+1)\}, \end{aligned} \quad (4)$$

$$\begin{aligned} \hat{x}^k(2m+1, 2n) &= \text{median}\{x^{k+1}(m, n-1), x^{k+1}(m, n), \\ &x^{k+1}(m, n+1), x^{k+1}(m+1, n-1), \\ &x^{k+1}(m+1, n), x^{k+1}(m+1, n+1)\}, \end{aligned} \quad (5)$$

$$\begin{aligned} \hat{x}^k(2m+1, 2n+1) &= \text{median}\{x^{k+1}(m, n), \\ &x^{k+1}(m, n+1), x^{k+1}(m+1, n), \\ &x^{k+1}(m+1, n+1)\}, \end{aligned} \quad (6)$$

$$d^{k+1}(m, n) = x^k(m, n) - \hat{x}^k(m, n), \quad (7)$$

where $\hat{x}^k(m, n)$ is an approximate image for scale k , $d^{k+1}(m, n)$ is a detailed image for scale $(k+1)$, $W_{i,j}^b$ is a window on center (i, j) of size $(2b+1) \times (2b+1)$, and usually $b=1$.

Donoho has already proved that $\text{MIPT}^{-1}(\text{MIPT}(x)) = x$ is true for the 1D case^[10]. And the same can be proved for the 2D case.

Following the 2D-MIPT, a lot of experiments are made from fifty typical images to verify the capability of transform which can separate detail and noise from halftoned version. And we want to find out the properties of halftoning noise for 2D-MIPT. Initially all of the images are halftoned by six kinds of ED kernels that are usually used in ED halftoning: Floyd-Steinberg, Burkers, Stucki, Sierra, Jarvis, and Stevenson^[1]. Then the preprocessed gray images which contain rich detail and halftoning noise are generated from their halftones by Gaussian LPF (3×3 , $\sigma = 0.6 - 0.8$) because 2D-MIPT cannot render halftones from $[0,1]$ to $[0,255]$. With these

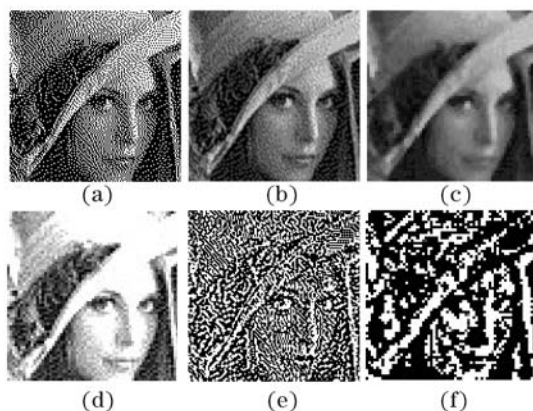


Fig. 2. Results of Lena for 2D-MIPT and FWT-7/9. (a) Floyd-Steinberg halftone; (b) preprocessed image filtered from (a) by Gaussian LPF; (c), (d) one-scale approximation for 2D-MIPT and FWT-7/9; (e), (f) details for 2D-MIPT on one and two scales.

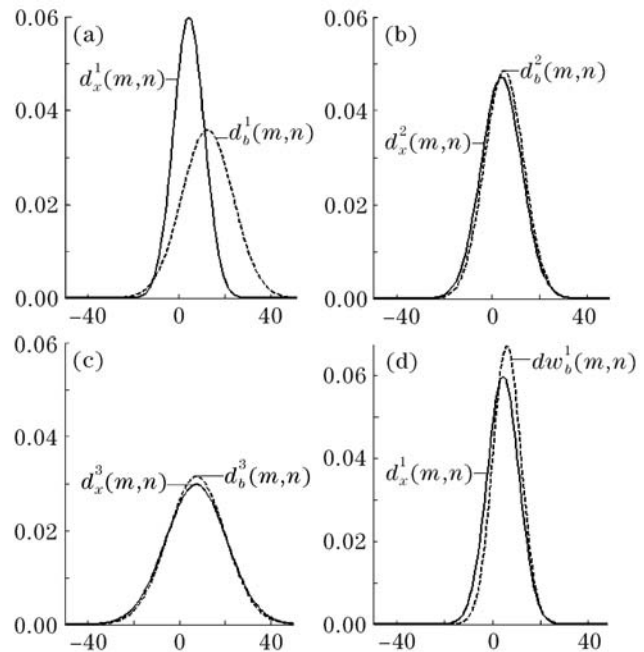


Fig. 3. PDF curves of Lena for 2D-MIPT on three scales. (a) – (c) PDF curves of details for originals and preprocessing halftones for 1 – 3 scales, solid lines are for $\{d_x^1, d_x^2, d_x^3\}$ and dashed lines for $\{d_b^1, d_b^2, d_b^3\}$; (d) Wiener filtering result of (a).

Table 1. Average Offsets of PDF for Fifty Originals and Their Preprocessing Halftones from One to Three Scales

ED Kernel	$d^1(m, n)$	$d^2(m, n)$	$d^3(m, n)$
Floyd	6.2611	0.7902	0.1642
Burkers	8.5849	1.2330	0.9047
Stucki	10.2667	1.5552	0.3857
Sierra	12.8083	1.8351	0.6255
Jarvis	13.9101	2.2777	0.8462
Stevenson	13.8132	6.2323	1.3129

preparations the original image $x(m, n)$ and its preprocessed one $b(m, n)$ are decomposed by 2D-MIPT on three scales. One of the results is shown in Fig. 2. The sequences $\{d_x^1, d_x^2, d_x^3, x^3\}$ and $\{d_b^1, d_b^2, d_b^3, b^3\}$ are obtained. Using the coefficients d_x^i and d_b^i , the curves of probability distribution function (PDF) on each scale are plotted, as shown in Fig. 3. Their average offsets of peaks are calculated, the results are listed in Table 1. In order to compare the separating capability with linear transform, the image is also decomposed by the wavelet function of FWT-7/9. The result is shown in Fig. 2(d). From these experiments the properties of ED noise for 2D-MIPT can be analyzed.

Property 1. As shown in Fig. 2, there is little noise in 1-scale approximation $x_b^1(m, n)$ and 2-scale detail $d_b^2(m, n)$ for 2D-MIPT. But the heavy noise remains on 1-scale approximation for FWT-7/9 because the wavelet decomposition is based on linear operator and has no adaptive capability to separate the nonlinear noise from ED halftone.

Property 2. From Fig. 3 and Table 1, the largest difference of PDF is found between $d_x^1(m, n)$ and

$d_b^1(m, n)$, and the others gradually go similar. It indicates that most of the halftoning noise is concentrated on detail of $d_b^1(m, n)$ for 2D-MIPT. And the power of halftoning noise is proportional to the size and shape of ED kernel.

Property 3. Focusing on the heavily noised detail of $d_b^1(m, n)$, several de-noising methods are employed such as finite impulse response (FIR) filter by spline function^[6], morphological filtering^[11], Wiener filtering and thresholding^[10,12]. The best result from Wiener filtering is shown in Fig. 3(d). The PDF differences and corrections between filtering and original are calculated in Table 2.

According to the above investigation and analysis, we use the nonlinear pyramid transform on multiple scales and de-noising as the wavelet case in Refs. [10 – 12]. A block diagram of the proposed inverse halftoning algorithm via 2D-MIPT is shown in Fig. 4. A small size of Gaussian LPF is applied on halftone b , and the pre-processed image x^0 is gotten which contains rich details and halftoning noise. Then the one-scale 2D-MIPT is selected to decompose x^0 into approximation x^1 and detail d^1 with *Properties 1* and *2* and efficiency of algorithm considered. Along with *Property 3*, a Wiener filter is employed to de-noise the distorted image d^1 , the cleaned detail dw^1 is obtained. Using inverse transform (IMIPT), the inverse halftoning image \hat{x}^0 will be reconstructed from dw^1 and x^1 . The result is reconstructed from median interpolating function, a fewer impulse noise will be introduced into \hat{x}^0 , so a median filter h is added for post-processing to generate the final result y^0 .

The ED kernels of Jarvis and Stevenson are bigger than others, and the latter is a hexagonal grid, so their halftoned version cannot render the gray level for $[1/2, 2/3]$. This will cause the visible disturbing artifact in halftoning patterns. If the inverse method cannot separate it very well, the artifacts will be processed as ill-edges. Considering this causation and *Property 3*, the new method adjusts all size of filters from 3×3 to 5×5 for the version which is halftoned by bigger or hexagonal ED kernel.

Table 2. Average Offsets and Corrections of PDF for Fifty Originals and Their 2D-MIPT Inverse Halftones on One Scale

ED Kernel	$d^1(m, n)$ Offset	$d^1(m, n)$ Correction
Floyd	3.4361	2.8250
Burkers	3.2729	5.3120
Stucki	3.4939	6.7728
Sierra	3.8158	8.9925
Jarvis	4.3380	9.5721
Stevenson	4.4285	9.4037

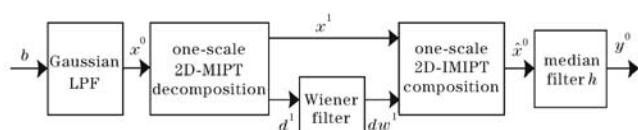


Fig. 4. Block diagram of the proposed inverse halftoning algorithm.

Table 3. PSNRs for Different Kinds of ED Kernel Halftones by Proposed Algorithm (dB)

ED Kernel	Peppers	Lena	Zelda
Floyd	31.0291	31.3512	33.7990
Burkers	30.6959	30.9326	33.5893
Stucki	30.0800	30.5117	33.1917
Sierra	29.8896	30.4056	33.0274
Jarvis	29.6751	30.1299	32.7299
Stevenson	28.0865	28.4065	30.7867

Table 4. Performance Comparison of Inverse Halftoning Algorithms in Terms of PSNR (dB)

Algorithm	Peppers	Lena	Zelda
LUT ^[2,3]	28.68	28.39	31.83
POCS ^[4]	27.59	28.64	—
MAP ^[5]	27.72	29.60	—
Nonlinear ^[6]	28.65	30.79	—
Wavelet ^[7]	28.56	30.38	—
Proposed	31.03	31.35	33.80

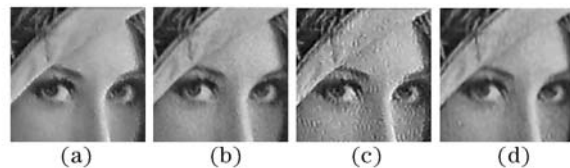


Fig. 5. Inverse halftoning results of Jarvis and Stevenson halftones for Wavelet^[7] and proposed algorithm. (a) Wavelet for Jarvis, PSNR = 27.0775 dB; (b) proposed for Jarvis, PSNR = 30.1299 dB; (c) Wavelet for Stevenson, PSNR = 23.0541 dB; (d) proposed for Stevenson, PSNR = 28.4065 dB.

Experiments were performed on Peppers, Lena, and Zelda in size of 512×512 pixels. First of all they were halftoned by six different kinds of ED kernels. Then the proposed method worked on these halftones, and their peak signal-to-noise ratios (PSNRs) are given in Table 3. We also compared our results with several previous inverse halftoning works such as look-up table (LUT)^[2,3], projection onto convex sets (POCS)^[4], MAP^[5], Nonlinear^[6], and Wavelet^[7]. All the PSNRs are shown in Table 4. The results for Jarvis and Stevenson halftones are specially shown in Fig. 5.

In conclusion, using nonlinear median operator and interpolating function, the multi-scale 2D-MIPT is given. With this transform, the ED halftoning noise can be separated better than the transform constructed by linear operator, and a new inverse halftoning algorithm is presented. The computational complexity and memory requirement of this method are very low because it only processes image in spatial field. Experiments demonstrate that the method shows efficient edge preserving ability, smooth inverse result, and robustness to different ED kernels. How to expand it for dither or color halftone is an interesting research in the future.

This work was supported by the Pre-Research Foundation of Ministries and Commissions

(No. 51416050205DZ0144), the Natural Science Foundation of Shaanxi Province (No. 2004F32), and the Scientific Research Program from the Education Department of Shaanxi Province (No. 04JK244). Y. Kong's e-mail address is kongyp@mail.xidian.edu.cn.

References

1. R. A. Ulichney, *Digital Halftoning* (MIT Press, Cambridge, 1987) p.233.
2. M. Mese and P. P. Vaidyanathan, in *Proceedings of IEEE International Symposium on Circuits and Systems* 517 (2000).
3. Y. Kong and P. Zeng, *Chin. J. Scient. Instrum.* (in Chinese) **25**, (Suppl. 4) 177 (2004).
4. P. W. Wong, *IEEE Trans. Image Processing* **4**, 486 (1995).
5. R. L. Stevenson, *IEEE Trans. Image Processing* **6**, 574 (1997).
6. M.-Y. Shen and C.-C. J. Kuo, *J. Visual Commun. Image Representation* **12**, 84 (2001).
7. Z. Xiong, M. T. Orchard, and K. Ramchandran, *IEEE Trans. Image Processing* **8**, 1479 (1999).
8. P. J. Burt and E. H. Adelson, *IEEE Trans. Commun.* **31**, 532 (1983).
9. G. Liu and W. Yang, *Acta Opt. Sin.* (in Chinese) **21**, 1336 (2001).
10. D. L. Donoho and T. P. Y. Yu, in *Proceedings of IEEE 31st Asilomar Conference Signals and Systems* 75 (1997).
11. W. Huang, D. Bi, B. Mao, and S. Ma, *Chin. J. Electron. Info. Technol.* (in Chinese) **26**, 1686 (2004).
12. S. Yin and W. Wang, *Chin. Opt. Lett.* **4**, 694 (2006).